Structural and Energetic Properties of RMX_3–NH_3Complexes

James A. Phillips,[1,*] Anna R. Ley, [1] Patrick W. Treacy,[1] Benjamin M. Wahl,[1] Brittany C. Zehner,[1] Kelling J. Donald,[2,*] and Samuel Gillespie[2]

1) Department of Chemistry and Biochemistry, University of Wisconsin - Eau Claire, 105 Garfield Ave, Eau Claire, WI 54701, United States.

2) Department of Chemistry, Gottwald Center for the Sciences, University of Richmond, 28 Westhampton Way, Richmond, VA 23173, United States.

* Authors to whom correspondence should be addressed:

J.A.P: Tel.: 715-836-5399; Fax: 715-836-4979; E-mail: phillija@uwec.edu
ORCID: James A Phillips 0000-0002-6697-7004

K.J.D: Tel.: 804-484-1628; Fax: 804-287-1897; E-mail: kdonald@richmond.edu
ORCID Kelling J. Donald: 0000-0001-9032-4225

ABSTRACT

We have explored the structural and energetic properties of a series of RMX_3–NH_3 (M=Si, Ge; X=F, Cl; R=CH_3, C_6H_5) complexes using density functional theory and low-temperature infrared spectroscopy. In the minimum-energy structures, the NH_3 binds axially to the metal, opposite a halogen, while the organic group resides in equatorial site. Remarkably, the primary mode of interaction in several of these systems seems to be hydrogen bonding (C-H--N), rather than a tetrel N$\rightarrow$M interaction. This is particularly clear for the $RMCl_3$–NH_3 complexes, and analyses of the charge distributions of the acid fragment corroborate this assessment. We also identified a set of metastable geometries in which the ammonia binds opposite the organic substituent in an axial orientation. Acid fragment charge analyses also provide a clear rationale as to why these configurations are less stable than the minimum-energy structures. In matrix-IR experiments, we see clear evidence of the minimum-energy form of CH_3SiCl_3–NH_3, but analogous results for CH_3GeCl_3–NH_3 are less conclusive. Computational scans of the M-N distance potentials for CH_3SiCl_3–NH_3 and CH_3GeCl_3–NH_3, both in the gas phase and bulk dielectric media, reveal a great deal of anharmonicity, and a propensity for condensed-phase structural change.

Keywords: molecular complexes, sigma holes, hydrogen bonding, tetrel bonding

Introduction

Interest in the structure and bonding of molecular complexes (also called "charge-transfer" or "donor-acceptor" complexes) has persisted for many decades. Most notably perhaps, Odd Hassel centered the lecture celebrating his 1969 Nobel prize on, "Structural Aspects of Interatomic Charge-Transfer Bonding".[1] A substantial review,[2] as well as several monographs[3-6] were published around that time as well, and in those initial works, the foundational ideas regarding the bonding interactions in these systems were outlined. More recent interest has been spurred, at least in part, by quantum-chemical investigations of molecular complexes,[7, 8] which have revealed more clearly the underlying nature of the interactions in these systems. In addition, these studies have led to the onset of newly-named sub-categories including "halogen" bonding,[9, 10] as well as "triel"[11] and "tetrel" bonding[12], for which the names acknowledge the geometries about the coordination centers, which in turn, affect the symmetry properties of the electron-deficient regions and acceptor orbitals. In all of these cases, however, the fundamental acid-base bonding motif (electron-donor to electron-acceptor) prevails.

One particularly comprehensive theoretical investigation of donor-acceptor systems appeared in the literature at about the time when the use of models incorporating electron correlation was becoming widespread,[7] and others followed in the years since.[8, 13] One notable outcome of these studies was the observation of a broad range of interactions, reflected in both strength and structure, spanning from long, weak, van der Waals-type contacts to much shorter and stronger cases, in-line with *bona fide* dative bonds. Moreover, one inescapable conclusion was that there was no fixed proportion of the electrostatic, charge-transfer, or dispersion contributions to the overall bonding in such complexes. Rather, the influence of each contribution is very sensitive to the type of complex and the specific pairs involved, and no single factor seems to correlate with strength in any over-arching manner.[7, 8, 13]

Another reason for the continued interest in these systems over the last two decades is a tendency for some complexes to undergo large changes in structure between the gas phase and various condensed-phase media.[14] The underlying principle is that any stabilizing medium – such as a

solvent, the solid-state, or even a noble gas matrix – may cause the donor-acceptor bond to contract relative to the gas phase, and there is a corollary distortion of the Lewis acid unit.[14, 15] For example, in the case of HCN–BF_3, the measured gas-phase B-N distance is 2.47 Å, but the bond shortens in the crystalline solid to a value of 1.65 Å, while the N-B-F angle opens by almost 14°.[16] Similarly, for FCH_2CN–BF_3, the predicted (B3PW91/aug-cc-pVTZ) structure has a B-N distance of 2.42 Å, but the value in the crystal structure is 1.64 Å.[17, 18]

In the Phillips group, we have been primarily concerned with the extent to which bulk media affect molecular complexes in this regard, and of particular interest are the effects of inert noble gas matrices: Solid argon, nitrogen, and neon.[15, 19] Much of our initial work focused on nitrile-BF_3 systems, which are classified as π-hole complexes,[20] due to the nature of the electron deficient region in the BF_3 acceptor, and, due to the three-coordinate acceptor moiety, the interactions in these systems are referred to as 'triel' bonds.[11] For FCH_2CN–BF_3, we observed a systematic red-shift for the B-F asymmetric stretching frequency across various media: gas-phase (BPW91/aug-cc-pVTZ) < Ne (s) < Ar(s) < N_2 (s).[21] These shifts spanned a range of about 250 cm^{-1}, and they were systematic, paralleling the charge-stabilizing ability of the medium (e.g., polarizability, dielectric constant, etc.), in a manner that was consistent with a progressive contraction of the B-N bond across these environments. Furthermore, computational scans of the interaction energy over a range of B-N distances revealed significant energetic changes that take place in bulk media along this reaction coordinate, and ultimately provided mechanistic insight into the experimentally-observed bond contractions.[15, 21, 22] In general, the complexes prone to substantial structural changes in the condensed-phase exhibit a notably flat donor-acceptor potential, with a global minimum at a long, essentially non-bonded distance, and only a gradual energy rise toward the inner wall, perhaps only a few kcal/mol over several tenths of an angstrom. Because the complexes are more polar at short distances, usually due to increased charge transfer and a greater degree of geometrical distortion in the acceptor unit, the solvation energy increases preferentially in the inner regions of the potential, and the minimum shifts to shorter values – if the curve is sufficiently flat, i.e., the energy range is comparable in magnitude to the energy of solvation.[19]

Subsequent studies of nitrogen-donor - MX_4 complexes (M=Si, Ge, Ti; X=F, Cl),[23-26] revealed some indication of condensed-phase structural changes, but overall, those were much less dramatic than the observations noted above for the B-N systems. One striking example was $CH_3CN–SiF_4$, for which theory predicted a long gas-phase Si-N distance of about 3.0 Å that would shorten by over 1.0 Å in low-dielectric media (□=5). However, no experimental evidence of this extraordinary structural change could be observed via low-temperature IR spectroscopy measurements.[23] More subtle effects were predicted for both nitrile-GeF_4 [23, 24] and imine-SiF_4 complexes,[26] but a complicating factor with these systems is that the stable reaction products that result from direct mixing of donor and acceptor are a 2:1 complexes (e.g.,$GeF_4(NCCH_3)_2$) with a 6-coordinate metal. This obscures any direct comparisons to the solid-state with regard to the analogous 1:1 system. Nonetheless, for $GeF_4(NCCH_2F)_2$, a 0.2 Å difference was noted between the Ge-N distances of the (predicted) gas-phase and (measured) solid state structures, and solid-state IR spectra are consistent with similar effects for $GeF_4(NCCH_3)_2$and $GeF_4(NCCH_2Cl)_2$.[24]

The Donald group has recently investigated a series of tetrel-type donor-acceptor complexes involving various MX_4 [27] and MXH_3 [28] acceptors, and showed that the sigma-hole concept is useful in rationalizing the structure and bonding in those systems.[29] The use of the term ‘sigma-hole’ has proliferated in the literature over the roughly thirteen years since its debut.[30] It describes the depletion in the charge density on atom Y outside the bonding region about the bond axis in an R-Y sigma bond, where R is an electron withdrawing substituent. If R is sufficiently electronegative relative to Y, a positive potential may arise in that sigma-hole region on Y around the extension of the R-Y bond, which is typically described as a ‘positive sigma hole’ or perhaps misleadingly as simply a ‘sigma-hole’. Donald et al. posit[27] that the presence of such positive potentials promote charge transfer into σ* orbitals on the acceptor such as SiF_4 in $F_4Si{\leftarrow}NH_3$, for example, The R-Y σ* orbital coincides typically with the extension of the R-Y bond axis such that both the electrostatic and changed transfer interactions are oriented in the same direction. Moreover, factors that stabilize one of those two contributions to the bonding – such as substituting for a more electron withdrawing R fragment – will strengthen both the electrostatic and change transfer contributions to the bonding by stabilizing the acceptor LUMO and strengthening the sigma hole. And, that is so, even if – as one article claimed quite recently[31] – the

electrostatic contribution to the bonding is more dominant in some forms of donor-acceptor interactions with strong sigma holes.

In this manuscript, we will report the structural and energetic properties of the ammonia complexes of a series of RMX_3 acceptors (M=Si, Ge; X=F, Cl; R = CH_3, C_6H_5), which are the monomethyl and monophenyl analogs of the MX_4 acids that we have studied previously. These systems are effective probes of the sigma-hole model, because they have distinctly different regions of positive potentials lying opposite the M-X and M-C bonds. These complexes are also of practical interest with regard to possible materials chemistry applications. The organic groups offer a means of linking these potentially "tunable" bonds to larger structures, wherein, a response to a change in chemical environment or other stimulus would allow one to modify the electronic properties. Thus, one could possibly induce a force within a chain, molecular wire, or other larger assembly. In this work, we report equilibrium structures and binding energies and M-N potentials curves for this series of complexes, as well as analyses of the fragment charge distributions. In addition, we will present results from IR spectra of cryogenic Ar matrices doped with NH_3 and CH_3SiCl_3 or CH_3GeCl_3 which are generally consistent with the weak interactions predicted for equilibrium structures of CH_3SiCl_3–NH_3, and to some extent, CH_3GeCl_3–NH_3 as well.

Materials and Methods

Computational Methods

All computations were performed using Gaussian 09 version B.0.1.[32] One set of structure searches was performed using a variety of methods including M06, M06-2X, ω-B97X-D, and MP2, with a series of basis sets ranging from 6-31G(d) to cc-pVTZ. In these searches, four basic coordination geometries were first considered; they were generated by placing the organic group and base in the axial or equatorial positions about a five-coordinate M center. Equilibrium conformations were then located by rotating the organic or NH_3 substituent accordingly upon the observation of imaginary torsional frequencies. In parallel, another set of geometry optimizations, at the M06/aug-cc-pVTZ level, was

carried out by considering each symmetric (C_s) conformation of the four geometrical isomers (16 in total for the complexes with R=CH_3). In the end, two types of stable structures were located; the "R-equatorial" forms, in which the NH_3 unit binds axially to the metal atom while the organic binds equatorially, and the "R-axial" forms, in which both organic and NH_3 bind axially to the metal.

For the reported structures, equilibrium geometries were obtained with convergence set criteria using the "opt=tight" condition and employed an ultra-fine integration grid. As a whole, the global minima were difficult to locate, presumably due to flat intermolecular potential surfaces, especially with regard to torsional motions, and some of the complexes exhibited several shallow minima. Often, it was essential to use force constants to guide the geometry optimizations (via the "opt=calcfc" option) in order to locate true minima which lacked imaginary frequencies. Ultimately, several of the final equilibrium structures lacked symmetry, and were identified by relaxing symmetry upon the observation of imaginary frequencies (usually for torsional motions). Also, in a few instances these results were double-checked using "opt=verytight". Ultimately, all the minimum-energy M06 structures were verified at the ω-B97X-D and M06-2X levels as well.

In order to find the most reliable method for predicting acid frequency shifts, which are essential for assigning and interpreting the low-temperature IR results,[15, 33] we conducted a validation study based on the experimental frequencies of CH_3SiCl_3 and CH_3SiCl_3, and employed five density functional theory methods[34] (M06,[35] B3LYP,[34] ω-B97X-D,[36] M06-2X,[35] and M05[35]), as well as MP2,[34] with the aug-cc-pVTZ[34] basis set. The neon-matrix frequencies for CH_3SiCl_3 and CH_3GeCl_3 that were obtained in this study were used as a validation benchmark. For both compounds, we found that M06 produced the lowest root-mean-squared error in predicting the six experimentally-observed vibrational modes for each acid fragment, thus we report the structural results from the M06/aug-cc-pVTZ calculations below.

A natural bond orbital analysis (NBO)[37] was carried out (also at the M06 level) for all fragments involve in these complexes, and we obtained computed point charges obtained from the natural population analysis,[38] as well as dipole moments. Electrostatic potential maps were generated using

the Gaussian View program by plotting the computed electrostatic potentials on the 0.001 au isodensity surface.

For CH_3SiCl_3–NH_3 and CH_3GeCl_3–NH_3, N-M potential energy curves were mapped in a point-wise manner at a series of fixed N-Si distances ranging from 1.5 to 4.5 Å for H_3N–$SiCl_3CH_3$ and 1.8 to 4.0 Å for H_3N–$GeCl_3CH_3$, respectively, in 0.1 Å increments. All degrees of freedom aside from fixed the N-Si distances were optimized at each point along these curves. For H_3N–$SiCl_3CH_3$, the method dependence was explored explicitly, by comparing results from □-B97X-D, M06, M06-2X, and M05, in addition to the CCSD energies of the M06 geometries (CCDS//M06), all with the aug-cc-pVTZ basis set. M06 was chosen as the primary method for subsequent investigations of the potentials, because it the energies agreed reasonably well with the CCSD values along the curve, and as noted above M06 was chosen for the reported structural results. Condensed-phase effects on the N-Si and N-Ge potentials of the R-equatorial configurations of CH_3SiCl_3–NH_3 and CH_3GeCl_3–NH_3 were explored by incorporating solvation free energies from the polarized continuum model (PCM)[9] into the M06 energies (i.e., PCM/M06/aug-cc-pVTZ), with dielectric constants ranging from 1.5 to 10.0, and other solvent parameters left at their default settings (i.e., for water).

Materials

Chemicals used in this study include trichloromethylsilane (EMD Millipore, >99%), trichloromethylgermane (Alfa Aesar, >97%) anhydrous ammonia (Praxair, >99.5%), and argon (Praxair, >99.999%). Prior to making gas mixtures for matrix-isolation experiments, $SiCl_3CH_3$ and $GeCl_3CH_3$ were purified via several freeze-pump-thaw cycles, but for bulk reactivity experiments, they were used without further purification. Gases were also used without further purification.

Bulk-Phase Reactivity

Direct, bulk-phase reactions between NH_3 and $SiCl_3CH_3$ or $GeCl_3CH_3$ were carried out by adding gaseous NH_3 to a sealed Schlenk tube (with a Teflon stopcock sidearm) containing neat liquid $SiCl_3CH_3$

or $GeCl_3CH_3$. First, 2-3 mL of liquid $SiCl_3CH_3$ or $GeCl_3CH_3$ was added to the tube, and it was capped with a rubber septum. Ammonia was the added via Teflon tube fitted with a hypodermic needle, which was punctured through the septum. The stopcock was opened slightly to also excess gas to escape prior to initiating the flow of NH_3. Solid white products formed immediately when the NH_3 entered the tube, and a slight temperature increase was noted. The NH_3 flow was continued until it had appeared that the reaction had completed. Both solid products were air stable, and showed no obvious signs of decomposition when the tubes were stored in a cabinet for several months. The products were insoluble in most solvents, and attempts to grow crystals via solvent diffusion were largely unsuccessful, aside from one sample that turned out to be crystals of NH_4Cl (s), presumably an elimination product. At this point, these solid products remain uncharacterized, but the efforts to identify and characterize them continue.

Matrix-Isolation Infrared Spectra

Matrix-Isolation IR spectra were obtained using a previously-described apparatus based on a Cyromech ST-15 optical cryostat. Gas mixtures (NH_3 in Ar, and CH_3SiCl_3 or CH_3GeCl_3 in Ar) were prepared in 2-liter glass bulbs (Chemglass) on a preparatory glass vacuum line. This system is maintained at a pressure of about 1×10^{-4} Torr using a glass diffusion pump (Chemglass AF-0330). Mixture concentrations ranged from 1/1600 to 1/400 (CH_3MCl_3/Ar or NH_3/Ar). For experiments involving both NH_3 and CH_3SiCl_3 or CH_3GeCl_3, matrix samples were deposited by flowing the mixtures through separate Teflon lines that merged immediately prior before entering the cryostat chamber by using a custom-designed, co-linear mixing flange. This is essential to prevent the formation of reaction products prior to deposition. For control experiments involving only NH_3 or CH_3SiCl_3 or CH_3GeCl_3, only one of these deposition lines was operated. In any event, the gas mixtures were ultimately condensed on a KBr window inside that cryostat vacuum chamber. Sample temperatures were controlled using a Scientific Instruments #9600 temperature controller and silicon diode located at the end of the refrigeration stage. Spectra were recorded using a Thermo Scientific Nicolet iS10 FT-IR with 1 cm^{-1} resolution. Typically, 400 were scans averaged (both background and sample) to obtain the final spectra. In most cases, two 60-minute depositions were run for 1-2 hours at 15-20K, and subsequently,

most samples were annealed for 60 minutes at 30 K. Spectra were recorded between depositions and after annealing.

Results and Discussion

Fragment Properties

For reference, we have displayed computed geometries (M06/aug-cc-PVTZ) for the acid fragments in Figure 1. For the most part, these overall geometries are retained in the complexes. The exceptions are CH_3GeF_3 and $C_6H_5GeF_3$, for which the corresponding complexes are significantly stronger than the other six. There are, however, some slight structural distortions that take place in the weaker complexes, that do shed some light on the nature of the interactions therein. The computed geometry of NH_3 has the expected C_{3v} structure with an N-H distance of 1.011 Å and an H-N-H angle of 107.0°.

As noted above, the M06 method was selected as the preferred method for the equilibrium structure results because it was it most accurately predicted the five measured (argon-matrix) vibrational frequencies of the commercially available acid fragments, CH_3SiCl_3 and CH_3SiCl_3. Experimental and theoretical (harmonic) frequencies, with methods as indicated and the aug-cc-pVTZ basis set, are listed in Tables 1 and 2 for CH_3SiCl_3 and CH_3GeCl_3, respectively; a scaling factor was not applied to the theoretical values. The RMS errors of the M06 predictions for CH_3SiCl_3 and CH_3GeCl_3 were 8.9 and 28.5 cm^{-1}, respectively. The latter error is notably larger, and as-a-whole the CH_3GeCl_3 predictions are less accurate. This may be due, in part, to isotopic composition; the predictions are strictly for ^{74}Ge isotopomer, while the measured frequencies reflect an average of five naturally-occurring isotopes of germanium. It is worth noting that we have also found M06 to be optimal in two recent studies of related MF_4 complexes,[24, 26] in which we employed a similar validation procedure. In

all cases, the goal is to make effective comparisons between the experimental and theoretical frequencies of the various complexes (*vide infra*).

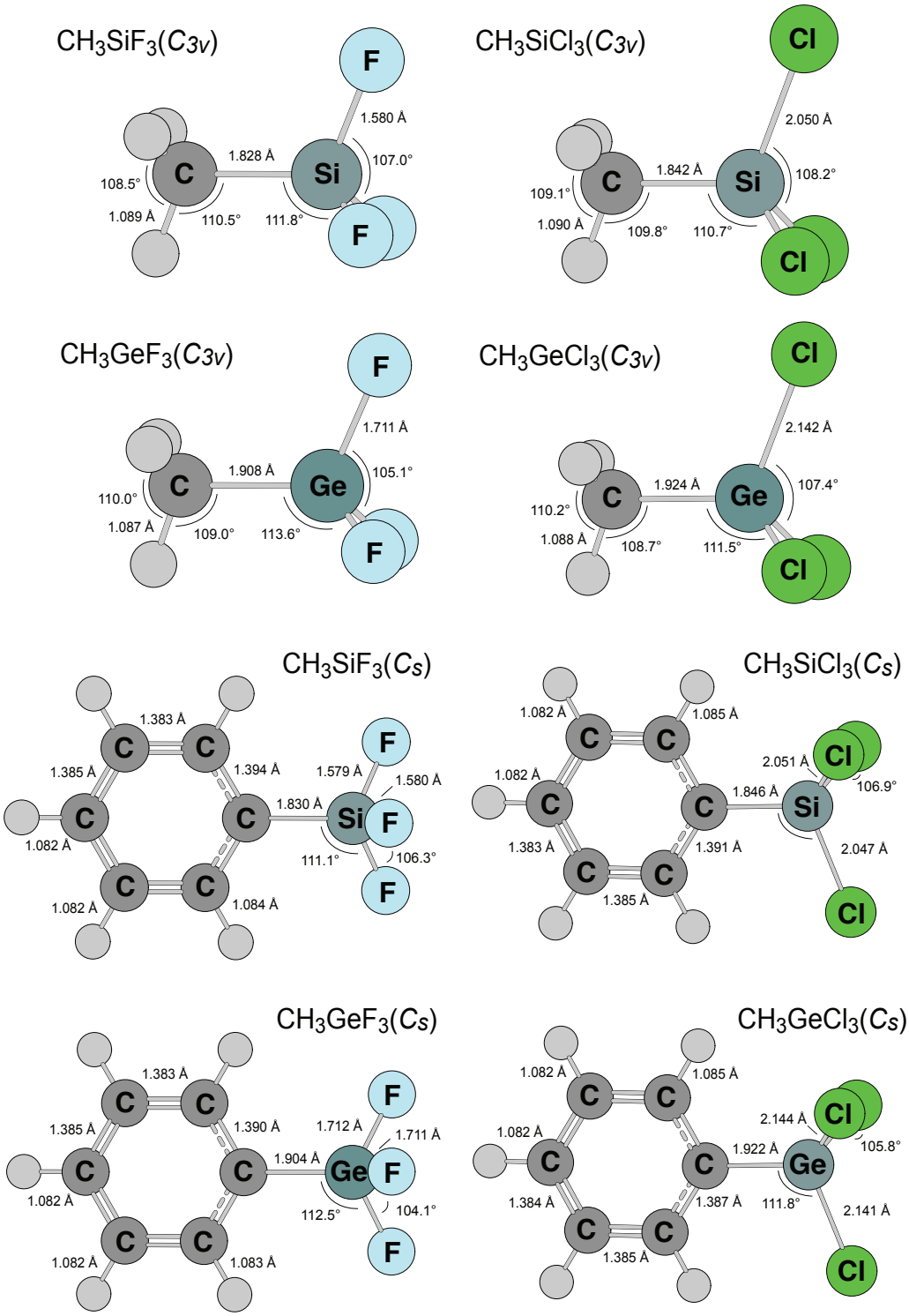

Figure 1: Computed M06/aug-cc-pVTZ equilibrium structures of the acid fragments, with symmetry as indicated.

Table 1: Measured and Calculated Frequencies[a] for CH_3SiCl_3

Mode \ Method [b]	B3LYP	ω-B97X-D	M05	M06	M06-2X	MP2	Exp.[c]
Si-Cl Asy. Stretch [d]	558	580	579	573	582	590	575
Si-C Stretch	745	768	745	759	778	774	761
CH3 Wag	829	827	813	800	816	823	799
CH3 "Umbrella" (SB) [d]	1299	1304	1264	1265	1291	1294	1266
CH3 Deformation (AB) [d]	1454	1456	1433	1422	1450	1466	1411
RMS Error	33.3	32.8	15.5	**5.8**	26.2	34.4	-

a) Units of cm^{-1}. b) Harmonic values from each stated method with the aug-cc-pVTZ basis set. c) Experimental values obtained in argon-matrix experiments; the uncertainty is about ± 1 cm^{-1}. d) For these frequencies there are two nearly-degenerate modes, symmetric (A') and asymmetric (A"), in the C_s point group, which are predicted to be split by 1 cm^{-1} or less and not resolved in our measurements. "AB" and "SB" signify "Symmetric Bend" and "Asymmetric Bend", respectively.

Table 2: Measured and Calculated Frequencies[a] for CH_3GeCl_3

Mode \ Method [b]	B3LYP	ω-B97X-D	M05	M06	M06-2X	MP2	Exp.[c]
Si-Cl Asy. Stretch [d]	415	431	430	434	441	452	434
Si-C Stretch	604	632	627	627	638	657	629
CH3 Wag	835	833	821	803	815	803	821
CH3 "Umbrella" (SB) [d]	1274	1287	1249	1241	1277	1272	1258
CH3 Deformation (AB) [d]	1455	1458	1434	1421	1454	1462	1407
RMS Error	61.2	60.0	**28.9**	**28.6**	52.3	68.2	-

a) Units of cm^{-1}. b) Harmonic values from each stated method with the aug-cc-pVTZ basis set. c) Experimental values obtained in argon-matrix experiments; the uncertainty is about ± 1 cm^{-1}. d) For these frequencies there are two nearly-degenerate modes, symmetric (A') and asymmetric (A"), in the C_s point group, which are predicted to be split by 1 cm^{-1} or less and not resolved in our measurements. "AB" and "SB" signify "Symmetric Bend" and "Asymmetric Bend", respectively.

Equilibrium Structures: Global Minima

As noted above, all four possible geometrical isomers were considered in both sets of structural searches, i.e., the four permutations that arise from placing the NH_3 subunit and R substituent (CH_3 or C_6H_5) in the axial or equatorial locations about the five-coordinate metal. We will utilize the "axial" and "equatorial" terminology that formally pertains to a trigonal-bipyramidal geometry about the metal, in spite of the fact that the acid fragments retain their near-tetrahedral geometries in most of the complexes. The exceptions are the $RGeF_3$ systems, but even in these cases the acid fragment is only partially distorted, and the geometries are intermediate between the tetrahedral and trigonal bipyramidal ideals. As a whole, these were difficult structure searches, and it is clear that the intermolecular potential surfaces in these systems are flat, especially with regard to angular and torsional degrees of freedom. Furthermore, additional meta-stable structures were identified in several cases.

In all cases, the two possible geometries in which the NH_3 was initially placed in an equatorial site were found to be unstable; they optimized to other structural forms. For each stable complex, the minimum-energy structure had the NH_3 bound in an axial manner, opposite a halogen, with the organic substituent in an equatorial position. We will refer to these configurations as 'methyl-equatorial' or 'phenyl-equatorial' as appropriate henceforth, or in general as the 'R-equatorial' geometries. The fact that these structures comprise the global minima are consistent with the sigma-hole model, which would predict that the strongest sigma-holes would reside opposite the halogens (*vide infra*). In addition, the structures with both the NH_3 and the organic substituent oriented axially, opposite one another, were also found to be stable, but also several kcal/mol higher in energy than the global-minimum, R-equatorial structures. We will refer to these meta-stable geometries as 'methyl-axial' or 'phenyl-axial' as appropriate henceforth, or in general as the 'R-axial' structures. The quasi-stability of these structures is also consistent with the sigma-hole model, the ammonia resides opposite the organic group, which also manifests a sigma-hole, but it is not as strong as that opposite the halogens (*vide infra*). In the unstable, NH_3-equatorial structures, there is no atom/group directly opposite the donor, and thus no sigma-hole interactions occur at these locations. However, it appears that tetrel-

like interactions between the NH_3 and the metal center are not the primary interactions in many of the minimum-energy geometries discussed below.

The minimum-energy methyl-equatorial and phenyl-equatorial structures of the CH_3MX_3–NH_3 complexes are displayed in Figures 2 and 3, respectively, and the corresponding thermochemical data are listed in Table 3. Overall, the M-N distances are extremely long in all cases except for CH_3GeF_3–NH_3 and $C_6H_5GeF_3$–NH_3. In fact, aside from these two systems, the other complexes are extremely weak, with long M-N distances ranging from 3.2 to almost 4.0 Å, near or sometimes exceeding the sums of the corresponding van der Walls radii (3.65 Å for Si--N and 3.66 Å for Ge--N). The binding energies range from 3.9 to 5.2 kcal/mol. In fact, for most of these systems, X=Cl in particular, it appears that any N-M tetrel-like interactions are missing or likely compromised; the acid geometries are nearly tetrahedral, and the NH_3 subunits are tilted towards a C-H bond on the R fragment in a manner that nearly aligns the C_3 axis of the ammonia with a C-H hydrogen. This seem to indicate C-H--N hydrogen bonding. In addition, in five of these six weaker systems, the exception being CH_3SiF_3–NH_3, the N--H distances are less than the sum of the N and H van der Waals radii (2.65 Å). Some additional observations pertaining to these interactions will be discussed below when the complexes are considered detail. As for the $RGeF_3$ systems, they exhibit evidence of moderately strong N$\rightarrow$Ge dative bonds, with binding energies of about 9 kcal/mol, and acid geometries that are significantly distorted, though the extent of this deformation is clearly intermediate. In addition, at about 2.3 Å, the Ge-N distances are a few tenths of an Angstrom longer than the sum of the Ge and N covalent radii (1.91 Å).

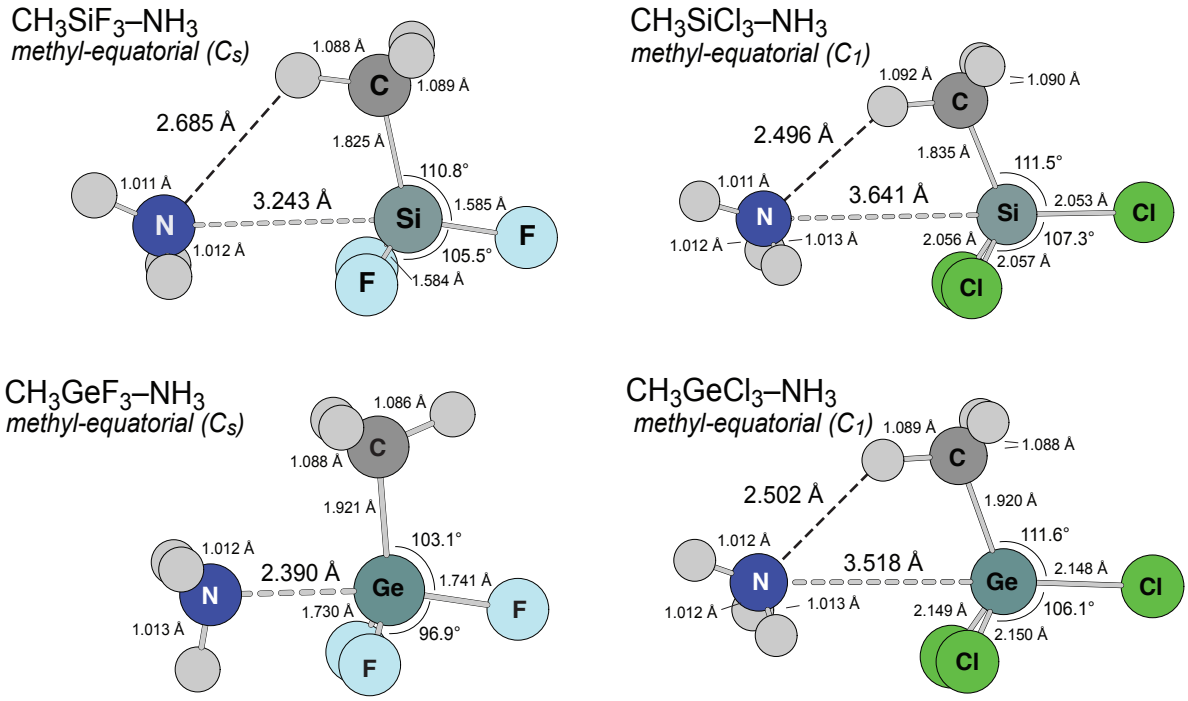

Figure 2: Minimum-energy, methyl-equatorial structures CH_3MX_3–NH_3 complexes via M06/aug-cc-pVTZ. The CH_3SiCl_3–NH_3 and CH_3GeCl_3–NH_3 complexes exhibit slight deviations from C_s symmetry; in addition to the minor bond length differences distances noted, the NH_3 subunit is tilted such that the upper-left N-H bond is rotated forward, out of the plane of the page.

Table 3: Thermochemical Data for R-Equatorial Isomers of RMX_3–NH_3[a]

Complex	ΔE[b]	ΔE_{ZPT}[b]	ΔH	ΔG
CH_3SiF_3–NH_3	-4.6	-3.7	-3.4	2.6
CH_3SiCl_3–NH_3	-4.2	-3.1	-2.9	3.7
CH_3GeF_3–NH_3	-8.9	-6.6	-7.1	1.6
CH_3GeCl_3–NH_3	-5.2	-4.1	-3.9	2.5
$C_6H_5SiF_3$–NH_3	-4.7	-3.3	-3.2	4.7
$C_6H_5SiCl_3$–NH_3	-3.9	-3.0	-2.6	4.2
$C_6H_5GeF_3$–NH_3	-9.4	-6.9	-7.5	3.6
$C_6H_5GeCl_3$–NH_3	-4.7	-3.6	-2.9	3.5

a) Units of kcal/mol. b) Energy difference between complex and sum of isolated fragments, "ZPT" refers to the zero-point-energy corrected value. c) ΔH and ΔG relative to isolated fragments at 298K.

The weaker three of the methyl-containing complexes displayed in Figure 2 adopt the same overall structural type. For CH_3SiF_3–NH_3, the NH_3 binds in a symmetrical manner, opposite one of the halogens (effectively axial), with the out-of-plane hydrogens eclipsing the equatorial halogens. CH_3SiCl_3–NH_3 and CH_3GeCl_3–NH_3 are similar, but these deviate slightly from C_s symmetry; the NH_3 is rotated by 11.1 and 16.5°, relative to that in the CH_3SiF_3–NH_3. One truly noteworthy feature in all three of these geometries for the weaker methyl-containing systems, is that the NH_3 is tilted as to direct its lone pair toward the adjacent, in-plane (for the acid fragment) hydrogen, suggestive of a weak hydrogen-bonding interaction.

The N--H distances for CH_3SiCl_3–NH_3 and CH_3GeCl_3–NH_3 are 2.495 and 2.502 Å, which are about 0.15 Å shorter than the predicted van der Waals contact distance (2.65 Å). In addition, the in-plane C-H bonds in the CH_3SiCl_3 and CH_3GeCl_3 subunits are very slightly elongated, by 0.002 and 0.001 Å, respectively. For H_3N–SiF_3CH_3, the N--H distance (2.685 Å) is about 0.2 Å longer and more comparable to the sum of the N and H van der Waals radii, while the Si-N distance (3.213 Å) is about 0.4 Å shorter the predicted van der Waals contact distance, and that in H_3N–$SiCl_3CH_3$. There is also no appreciable elongation of the in-plane C-H bond. These observations seem to indicate that a weak, N-Si tetrel interaction accompanies any H-bonding, certainly more so than in CH_3SiCl_3–NH_3. It seems also possible that these weaker methyl-containing complexes are further stabilized by favorable electrostatic interactions between the NH_3 hydrogens and the halogens they eclipse (or nearly) on the acid subunit. These H--X distances are about 2.8 to 3.0 Å, but if these interactions were appreciable strong it would conflict with the observation that the NH_3 is nearly free rotor in these complexes.

By contrast, CH_3GeF_3–NH_3 exhibits some key structural differences from its three weaker counterparts, beyond a fairly short Ge-F distance and a significantly distorted coordination geometry about the Ge. In this case, the NH_3 is in a staggered conformation relative to the GeF_3 framework, while the CH_3 and GeF_3 are eclipsed (the free CH_3GeF_3 structure is staggered, see Figure 1). The upshot of this is that there is no C-H--N interaction, and a Ge$\rightarrow$N dative bond is the primary interaction. The acid geometry is only partially distorted, however, the bond angles displayed in Figure 2 (96.9° and 103.1°) lie between the values for the ideal tetrahedral and trigonal bipyramidal geometries. This

suggests a tetrel bond of intermediate strength, consistent with the binding energy value relative to other systems, a Ge-N distance that is fairly short yet still about 0.3 Å longer than the sum of the covalent radii.

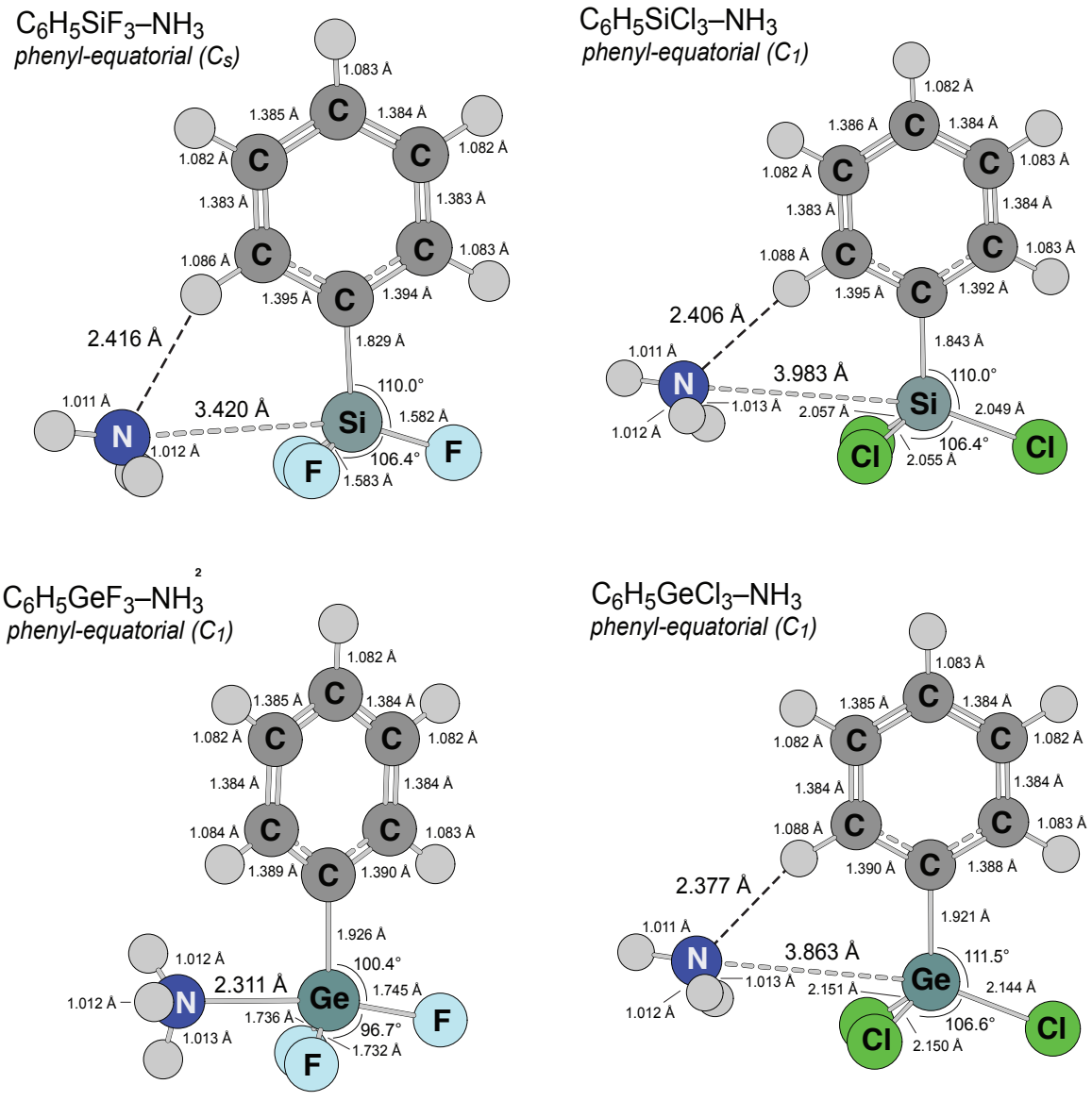

Figure 3: Minimum-energy, phenyl-equatorial structures $C_6H_5MX_3$–NH_3 complexes via M06/aug-cc-pVTZ. The $C_6H_5SiCl_3$–NH_3 and $C_6H_5GeCl_3$–NH_3 complexes exhibit slight deviations from C_s symmetry; in addition to the minor bond length differences noted, the NH_3 subunit is tilted such that the upper-left N-H bond is rotated forward, out of the plane of the page.

The detailed aspects of the structures of the phenyl complexes (Figure 3) largely parallel the structures of their methyl counterparts, but there are some key differences. Again, for the three relatively weak systems, $C_6H_5SiF_3$–NH_3, $C_6H_5SiCl_3$–NH_3, and $C_6H_5GeCl_3$–NH_3, the out-of-plane NH_3 hydrogens are approximately eclipsed with the corresponding halogens. Specifically, $C_6H_5SiF_3$–NH_3 is symmetric and the H's are essentially eclipsing the halogens. However, like CH_3SiCl_3–NH_3, and CH_3GeCl_3–NH_3 above, the NH_3 subunits in $C_6H_5SiCl_3$–NH_3 and $C_6H_5GeCl_3$–NH_3 are rotated about the torsional coordinate by 18° and 14°, respectively. In addition, for $C_6H_5SiF_3$–NH_3, $C_6H_5SiCl_3$–NH_3, and $C_6H_5GeCl_3$–NH_3, the NH_3 is tilted toward the adjacent C-H bond of the phenyl ring in a manner that suggests a weak H-bonding interaction (C-H--N). However, the distances in all three of these weaker phenyl-containing systems are much shorter than those of their methyl counterparts. All are near 2.4 Å, which about 0.4 Å shorter than the predicted van der Waals contact distance. This, together with the extremely long Si-N and Ge-N distances indicates that H-bonding likely comprises the primary interactions in these systems. For $C_6H_5SiCl_3$–NH_3 and $C_6H_5GeCl_3$–NH_3, the N-Si and N-Ge distances (3.983 and 3.863 Å, respectively) are over 0.2 Å *longer* than the predicted van der Waals contact distances (3.65 Å). Also, we note that the situation with $C_6H_5SiF_3$–NH_3 seems to parallel the other weak phenyl complexes, rather than its methyl counterpart in Figure 2. Here is N--H distance (2.416 Å) is comparable to those in the $C_6H_5MCl_3$ systems, and is again on par with sum of the N and H van der Waals radii. This, together with an N-Si distance that is about 0.2 Å longer than its methyl counterpart, and perhaps a bit less distortion of the acid subunit, suggest that H-bonding along the C-H--N linkage may be the primary interaction here as well. It is also worth noting that we did locate secondary minima for $C_6H_5SiF_3$–NH_3, $C_6H_5SiCl_3$–NH_3, and $C_6H_5GeCl_3$–NH_3 that had shorter M–N distances, and lacked any such H-bonding interaction, due to a tilt in the phenyl ring which rendered the C-H bond inaccessible. However, these geometries were all about a kcal/mol higher in energy than the structures displayed in Figure 3.

The fairly strong $C_6H_5GeF_3$–NH_3 complex is the outlier relative to its phenyl-containing counterparts, and its structure parallels that of its methyl analog, with a short Ge-N distance (2.311 Å), and a moderately large binding energy (9.4 kcal/mol). The acid fragment is significantly distorted, with bond angles of 96.7 and 100.4°, intermediate between the ideal tetrahedral and trigonal bipyramidal values,

once again suggesting an interaction best described as “intermediate”. Also, the NH_3 is only approximately staggered with respect to the acid fragment; it is tilted by about 23° (such that the lower N-H bond in Figure 3 points into the plane of the page). In addition, the phenyl ring is tilted by about 37° relative to the plane defined by the F_{axial}-Si-C_a linkage (the left side of the ring as pictured in Figure 3 would extend out of the plane of the page).

Despite the variability in the modes of interaction across this family of systems, there are some reasonably clear general trends in strength. Two general observations are that the binding energies are significantly offset by the zero-point energy corrections, and in addition, the Gibbs energy changes for the formation of the complexes are all positive. As a whole, the Ge-containing complexes are stronger than their silicon analogs, by about 1 kcal/mol in the case of the X=Cl compounds, and by 4-to-5 kcal/mol in the case of the X=F compounds. Similarly, the fluorine-containing systems are stronger than their chloro counterparts by about 0.5 to 1.0 kcal/mol in the case of M=Si, and by about 4-to-5 kcal/mol in the case of M=Ge. The effect of the R-group is quite subtle, and manifests differences in binding energy of only 0.1 to 0.5 kcal/mol. In the case of the X=F systems, the R=C_6H_5 complexes are somewhat more strongly bound, and in the case of the X=Cl systems the R=CH_3 complexes are slightly stronger.

These strength (i.e., binding energy) trends however, do not always parallel structural data such as the M-N distances in a manner expected for donor-acceptor systems - this is further evidence that weak H-bonding makes significant contributions to the overall interaction energies. Some key structural parameters for these complexes (and again, their R-axial counterparts), are summarized in Table 4. Case in point here are the X=Cl systems, in which the R=C_6H_5 analogs have significantly longer M-N distances than their R=CH_3 counterparts, but have larger binding energies, and much shorter C-H--N distances. These observations are quite consistent with the predominance of the H-bonding interactions over any sort of tetrel-bonding interaction between the NH_3 and the metal center. However, the fact that both M=Ge systems have shorter M-N distances than their M=Si analogs does argue for some sort of composite interaction. A similar situation arises upon a comparison of CH_3SiF_3–NH_3 and $C_6H_5SiF_3$–NH_3, in which the binding energy of the former is smaller (albeit by only 0.1

kcal/mol), but its Si-N distance is a full 0.2 Å shorter. But this too can be rationalized by considering H-bonding interactions within the C-H--N linkage, which seem to be secondary for CH_3SiF_3–NH_3 (shorter N-Si distance, smaller binding energy) but more dominant in $C_6H_5SiF_3$–NH_3 (longer N-Si distance, large binding energy).

One additional point of comparison is how the strengths of these complexes compare to their MX_4 counterparts, an illustration of how replacing a single halogen with an organic substituent affects acceptor strength. The M06/aug-cc-pVTZ binding energies of the NH_3 complexes of SiF_4, $SiCl_4$, GeF_4, and $GeCl_4$, which are exclusively tetrel bonded, are 9.4, 3.1, 19.7, and 5.8 kcal/mol, respectively. Among these, the SiF_4 and GeF_4 are relatively strong, and the latter most likely provides a reliable benchmark for a strong tetrel bond. In addition, they are substantially, stronger than their MF_3R counterparts, by about 5 kcal/mol and about 10 kcal/mol, for H_3N–SiF_4 and H_3N–GeF_4, respectively. This indicates that the addition of the R-group substantially reduces the Lewis acidity of these M=F compounds. However, the situation with H_3N–$SiCl_4$ and H_3N–$GeCl_4$ is quite peculiar. In these cases, the binding energies are within about 1 kcal/mol of their MCl_3R counterparts, and in fact, the binding energy of H_3N–$SiCH_3Cl_3$ just slightly *exceeds* that of H_3N–$SiCl_4$. One factor is apparently that the X=Cl compounds are much weaker acceptors than their X=F counterparts, but any trend may also be obscured by difference in the nature of the interactions in the MCl_4 and MCl_3R complexes – tetrel vs H-bonding, respectively.

Metastable 'R-Axial' Structures

In addition to the global-minimum R-equatorial structures, we also identified a set of metastable R-axial structures, which are depicted in Figures 4 and 5 for the methyl and phenyl compounds, respectively, and corresponding thermochemical data are presented in Table 4. These structures may be inaccessible from an experimental standpoint, but they do illustrate the applicability of the sigma-hole model to these compounds with distinctly different bonding sites. Furthermore, as we move forward with this line of research, we will be seeking complexes for which the R-axial configuration is most stable, and the sigma-hole concept will guide us in that effort. In any event, these R-axial structures are all true minima with all real frequencies. To some extent these structures fall into two

classes, those with fairly short or fairly long M-N interaction distances. In fact, the CH_3SiCl_3–NH_3 and CH_3GeCl_3–NH_3 systems exhibit two distinct R-axial structures distinctly different M-N bond distances, a phenomenon we have encountered before in our studies of nitrile - BCl_3 complexes.[39, 40] For the most part, these structures lie 2-3 kcal/mol above the respective R-equatorial structures. The exceptions are the short-bond forms of the $RMCl_3$–NH_3 complexes, which lie about 4 to 6 kcal/mol above their R-equatorial counterparts.

The structures with relatively long M-N distances are displayed on the left in Figures 4 and 5, and these include the "long-bond" forms of the $RSiCl_3$–NH_3 and $RGeCl_3$–NH_3 systems, as well as the $RSiF_3$–NH_3 complexes. For the most part, these structures reflect weak NM tetrel interactions, in which the acid fragments remain largely undistorted. For CH_3SiCl_3–NH_3 and CH_3GeCl_3–NH_3, the M-N distances systems are about 0.15 to 0.20 Å shorter than the expected van der Waals contact (3.65 Å for Si--N, 3.66 Å for Ge--N), and binding energies are -2.5 and 2.0 kcal/mol respectively. For $C_6H_5SiCl_3$–NH_3 and $C_6H_5GeCl_3$–NH_3 appear to be slightly weaker systems; the M-N distances are longer, very near the predicted van der Waals contact value, and the binding energies are less (1.7 and 2.0 kcal/mol, respectively). Also, in these systems, the NH_3 subunit it tiled in a manner that seems to align its dipole with one of the M-Cl bonds, thereby disfavoring the tetrel interaction. The $RSiF_3$–NH_3 complexes exhibit N-Si distances near 3.0 Å, about 0.5 Å less than the predicted van der Waals contact, and binding energies of about 2.5 kcal/mol. In addition, these distances are 0.2 and 0.4 Å shorter than in the global minimum RE structures for the methyl and phenyl complexes, respectively, in spite of the binding energies that are lower by 2 kcal/mol. The reason for this is not clear, but it is consistent with a significant H-bonding contribution to the interaction energies in the R-equatorial forms of these complexes.

The structures with relatively short M-N distances are displayed on the right in Figures 4 and 5, and these consist of the $RGeF_3$–NH_3 complexes, and the short-bond forms of the $RSiCl_3$–NH_3 and $RGeCl_3$–NH_3 systems. The $RGeF_3$–NH_3 structures are quite similar, and reflect moderately strong N$\rightarrow$M tetrel interactions with fairly short Ge-N distances (2.153 Å), a significant degree of distortion in the acid fragments, and moderately large binding energies (7.9 kcal/mol). Like their silicon counterparts, the

M-N distances are shorter than in the R-equatorial forms, in spite of the weaker binding. The short-bond forms of the $RSiCl_3$–NH_3 and $RGeCl_3$–NH_3 complexes exhibit notably short M-N bonds, over 1.0 Å shorter than their long-bond counterparts, and a significant distortion of the acid fragments. However, each of these short-bond structures is higher in energy than its long-bond analog, though in the case of CH_3GeCl_3–NH_3, the difference is only 0.6 kcal/mol. In fact, $C_6H_5SiCl_3$–NH_3 lies 1.7 kcal/mol above the separated fragments.

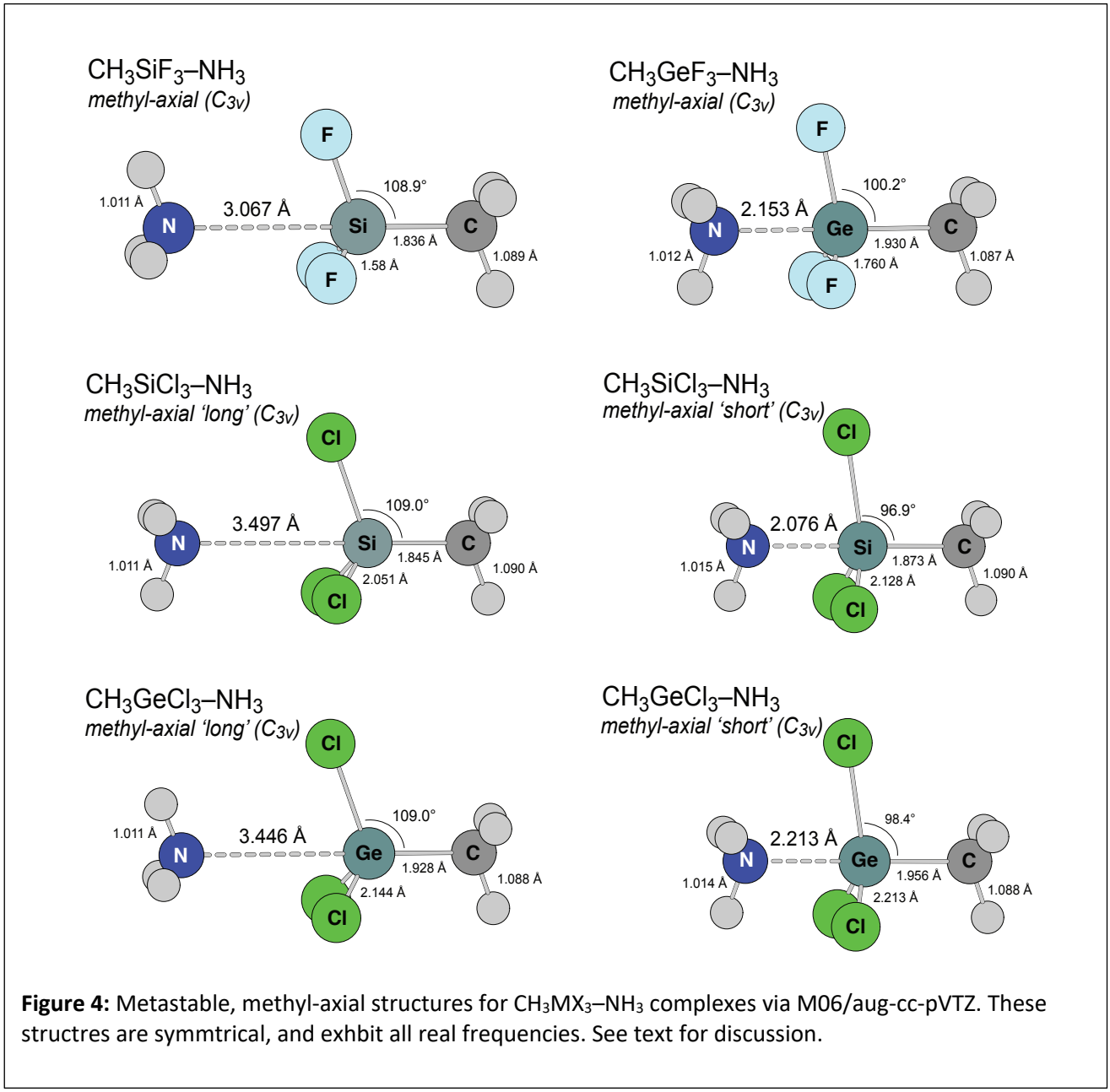

Figure 4: Metastable, methyl-axial structures for CH_3MX_3–NH_3 complexes via M06/aug-cc-pVTZ. These structres are symmtrical, and exhbit all real frequencies. See text for discussion.

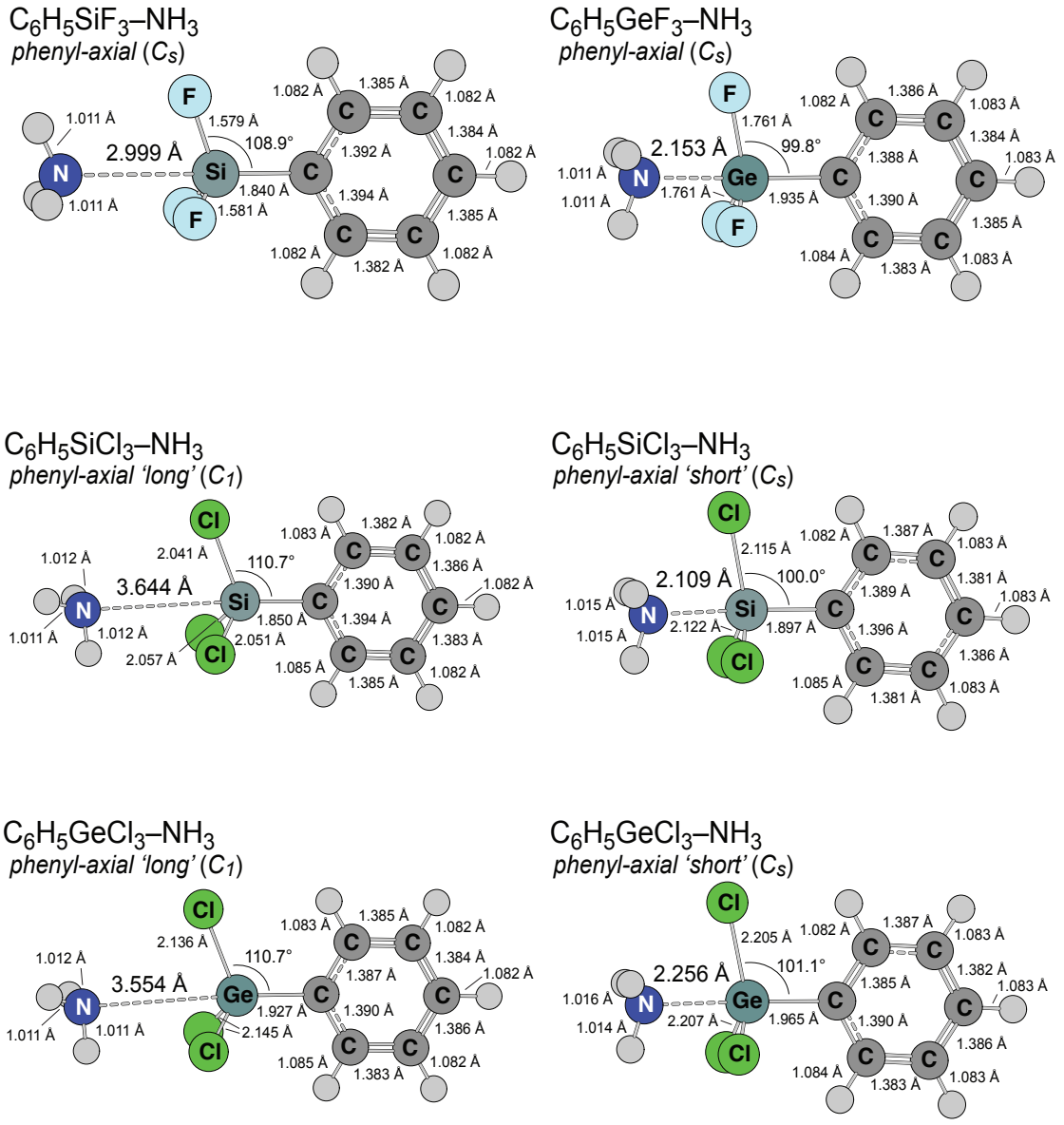

Figure 5: Metastable, phenyl-axial structures for $C_5H_6MX_3$–NH_3 complexes via M06/aug-cc-pVTZ. For the long-bond forms of $C_6H_5MCl_3$–NH_3 (*lower left*), the NH_3 is tilted inward in a manner that partailly aligns its C_3 axis with the M-Cl bond projecting into the page.

Table 4: Thermochemical Data for R-Axial Isomers of RMX_3–NH_3[a]

Complex	ΔE[b]	E_{rel}[c]	ΔE_{ZPT}[b]	ΔH [d]	ΔG [d]
CH_3SiF_3–NH_3	-2.5	2.2	-1.7	-1.3	4.4
CH_3SiCl_3–NH_3 *(short)*	-0.1	4.2	3.5	2.4	13.6
CH_3SiCl_3–NH_3 *(long)*	-1.7	2.5	-0.9	-0.4	6.2
CH_3GeF_3–NH_3	-7.9	1.0	-5.2	-5.9	4.3
CH_3GeCl_3–NH_3 *(short)*	-1.4	3.8	1.6	0.8	11.5
CH_3GeCl_3–NH_3 *(long)*	-2.0	3.2	-1.4	-0.8	4.9
$C_6H_5SiF_3$–NH_3	-2.6	2.0	-1.7	-1.4	4.8
$C_6H_5SiCl_3$–NH_3 *(short)*	1.7	5.6	4.8	3.9	14.3
$C_6H_5SiCl_3$–NH_3 *(long)*	-1.7	2.2	-0.9	-0.5	6.2
$C_6H_5GeF_3$–NH_3	-7.9	1.5	-5.1	-5.8	5.7
$C_6H_5GeCl_3$–NH_3 *(short)*	-0.2	4.5	2.7	2.0	12.3
$C_6H_5GeCl_3$–NH_3 *(long)*	-2.0	2.7	-1.2	-0.3	4.8

a) Units of kcal/mol. b) Energy difference between complex and sum of isolated fragments, "ZPT" refers to the zero-point-energy corrected value. c) E_{rel} is the energy relative to the corresponding R-*equatorial structure. d*) ΔH and ΔG relative to isolated fragments at 298K.

Charge Analyses

The seemingly peculiar aspects of the bonding in these systems, including the apparent preference for weak H-bonding over N→M tetrel interactions, are laid bare in an assessment of the charge distribution across this full series of RMX_3–NH_3compounds. Table 5 displays key parameters related to the charge distributions of the acid fragments, including: NBO charges at the M and X centers, dipole moments, and maximum values of the electrostatic potential on the isodensity surfaces (0.001 au) in the sigma-hole regions opposite the X and R substituents.

Table 5: Key Charge Distribution Parameters for Acid Fragments[a]

Fragment	NBO Charge / e			μ / D	Maximum ESP / au[b]	
	H	M	X		*M-R	*M-X
CH_3SiF_3	0.25	Si: 2.36	F: -0.64	2.45	0.029	0.044
$SiCl_3CH_3$	0.25	Si: 1.46	Cl: -0.36	1.94	0.009	0.027
CH_3GeF_3	0.25	Ge: 2.23	F: -0.64	3.8	0.021	0.055
CH_3GeCl_3	0.25	Ge: 1.36	Cl: -0.36	2.63	0.009	0.034
$C_6H_5SiF_3$	0.20(1)	Si: 2.38	[c] F: -0.64 -0.64	3.2	0.028	0.039
$C_6H_5SiCl_3$	0.20(1)	Si: 1.49	[d] Cl: -0.35 -0.36	2.71	0.006	0.016
$C_6H_5GeF_3$	0.20(1)	Ge: 2.06	[c] F: -0.64 -0.67	4.94	0.015	0.049
$C_6H_5GeCl_3$	0.20(1)	Ge: 1.39	[d] Cl: -0.35 -0.35	3.6	0.005	0.022

a) For NH_3, the point charges are -1.06e, and 0.35e for N and H respectively, and μ = 1.49 D. b) The maximum electrostatic potential observed in sigma-hole region (on the 0.001au isodensity surface of MX_3R) on M opposite the M-R or M-X bonds as indicated. For NH_3 the potential extremum is -0.059 au at the lone pair on N. c) Top: 30° dihedral angle; bottom: 90° dihedral angle. d) Top: 0° dihedral angle; bottom: 60° dihedral angle.

One clear thing to note is that the computed point charges at M and X are relatively insensitive to the identity of R. The exception is CH_3GeF_3 relative to $PhGeF_3$, in which the metal center is slightly less positive in the case latter case (2.06e vs. 2.23e), an indication that the phenyl group does release some additional electron density relative to methyl. In addition, charge saturation appears to be achieved by the F and Cl centers on both Si and Ge compounds; the charges on F and Cl are consistently -0.64*e* and -0.35(1)*e*. However, the charge transfer from M to the X centers is noticeably higher for X = F than for X = Cl, such that the M centers in the fluoride molecules have a higher positive charge, by roughly 0.7e to 0.9e. In addition, the dipole moments of the fluorides are higher as well, by about 0.5 D for M = Si, and by 1.2 to 1.3 D for M = Ge.

Again, as was noted above, the identity of R has little or no effect on the charges at the M and X centers, $RGeF_3$ compounds notwithstanding, but there are some differences between the methyl and phenyl systems. For one, the phenyl compounds have much larger dipole moments, by roughly 0.8 to 1.0 D. In addition, the sigma holes (both M-R and M-X) tend to be slightly stronger in the methyl cases, as indicated by the maxima on the electrostatic potential surfaces. For the methyl-fluoro compounds, the maxima are about 0.005 au larger in magnitude than their phenyl counterparts. For the methyl-chloro compounds, the maxima are about 0.01 au larger in magnitude than their phenyl counterparts. However, these differences are minor compared to those manifested by the identity of the X or M centers.

Above all else, it is the identity of the halogens that manifests the most significant difference in the charge distribution parameters of the acid fragments, and in turn, the most significant difference in the strength of the coordinate bond to NH_3. For instance, the maximum potential at Ge opposite the Ge-Cl bond (~ +0.005 au) is a full order of magnitude smaller than maximum potential at Ge opposite the Ge-F sigma holes (~ +0.049 au). Thus, any potential consequence of differences in the electron donating abilities of methyl and phenyl, for instance, are rendered negligible by the dominant electron withdrawing power of the geminal halogen substituents on the common M center. In fact, the potentials on M opposite both the M-X and M-R bonds are significantly intensified by replacing Cl by F, and this far exceeds the effect due to R. As a whole, however, the potentials M opposite the M-C bonds for both phenyl and methyl are substantially lower than those opposite the M-X bonds, even when the methyl substituent induces a small but consistently more positive potential than phenyl. An apparent consequence of the disparity in the strengths of the sigma holes opposite the M-X and the M-R bonds is that complexes with the base axial to the M-R bonds are consistently less stable than the alternative systems with the base axial to the M-X bond. This is so even though the latter systems have consistently longer M-N contacts, which is explained, in part, by the prevalence of hydrogen bonding in some of the R-equatorial structures. However, even for $H_3N–GeF_3CH_3$, the R-equatorial geometry with NH_3 axial to the Ge-F bond has a Ge-N distance that is over 0.20 Å longer, but the binding energy exceeds that that if the R-axial structure by 2.0 kcal/mol.

Maps of the electrostatic potentials for the fluorine-containing acid fragments – plotted on a common scale for the case of the most extreme potentials – are shown in Figure 6. The structures are oriented such that the halides are at the top, with on pointing into the plane of the paper. The structures are tilted such that the slightly positive potentials opposite the R groups are visible at the top of the maps, while those due to the halide (on the backside of each structure) are front-and-center (*see annotations*). Above, we noted a remarkable observation, that for most of the weaker, R-equatorial structures, a C-H--N hydrogen-bonding interaction seems to predominate over direct coordination to the metal center. These potential maps in Figure 6 relieve us of any anxiety about this outcome. Certainly, for the chlorine-containing fragments (*right*), which are most clearly H-bonded in the R-equatorial forms, the potentials on the H centers are the most positive (blue); more so than either sigma-hole region. At the other extreme, CH_3GeF_3 and $C_6H_5GeF_3$ (*bottom left*) exhibit distinctly positive regions for the sigma-holes opposite the Ge-F bond, and these fragments form moderately strong N→Ge tetrel bonds with NH_3. The CH_3SiF_3 and $C_6H_5SiF_3$ cases are less clear, as the blue (positive) regions about the hydrogens and the *M-X sigma hole are comparable, perhaps slightly favoring the latter. In turn, the interactions with the NH_3 subunit in the complexes are less distinct, with the bond axis of the NH_3 fragment pointing between the C-H bond and the metal center, perhaps a compromise between the tetrel (N→Si) and H-bond (C-H--N) interactions.

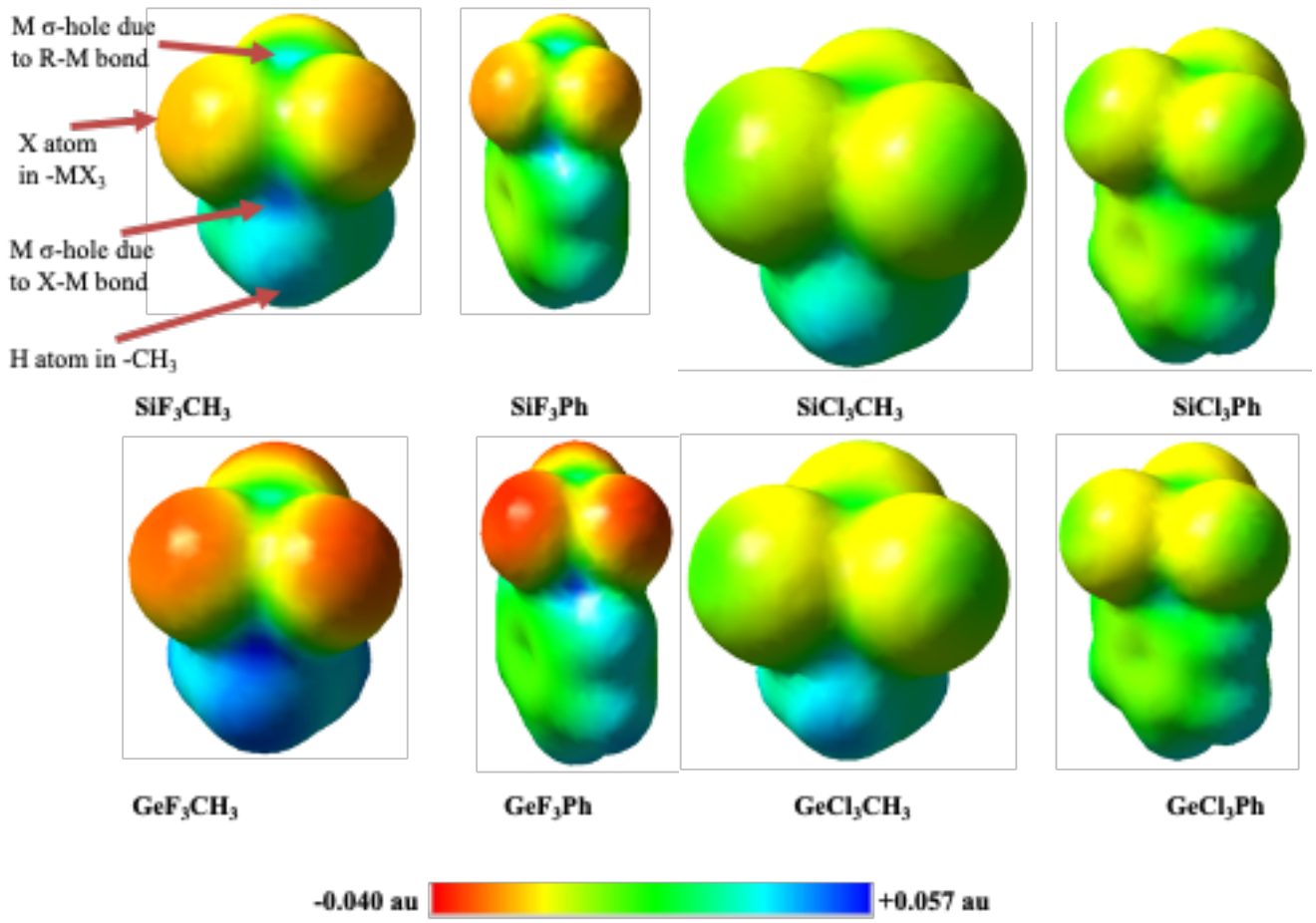

Figure 6: Electrostatic potential maps for the acid fragment (MX_3R) systems. The maps are all plotted on a common scale (spanning potentials of +0.0566 au (blue) to -0.0400 au (red)) on the 0.001 au isodensity surface.

Matrix IR Spectra

We obtained infrared spectra of cryogenic argon matrices seeded with NH_3 and CH_3SiCl_3 or CH_3GeCl_3, and ultimately found that the observed patterns of the product bands (those that are observed only the presence of both complexes subunits) were consistent with the presence of the methyl-equatorial form of CH_3SiCl_3–NH_3, but less conclusive in the case of CH_3GeCl_3–NH_3. We note here that these spectra were difficult to interpret due to weak product-band signals that were shifted only slightly from the corresponding fragment bands. This was particularly problematic in the case of CH_3GeCl_3 experiments, because of the presence of five naturally abundant Ge isotopes, which significantly broadens most of the fragment bands. Typically, matrix-IR spectra are assigned though a meticulous analysis of peak areas, undertaken to ensure that assigned product bands exhibit consistent relative intensities across a range of conditions. Here, the product bands reported were only observed in a narrow range of near-optimal conditions, and peak area measurements were unreliable due overlap with the relatively strong fragment bands. However, the validated M06 frequency predictions make a compelling case for the presence of the RE forms of the complexes, especially for CH_3SiCl_3–NH_3, even in the absence of rigorously-confirmed band assignments.

In matrices seeded with NH_3 and CH_3SiCl_3, we observed product bands at 566/567, 765, 810/816, and 1048 cm^{-1}, the first three of which are shifted only slightly from the following peaks observed for the CH_3SiCl_3 fragment: The Si-Cl asymmetric stretch at 575 cm^{-1}, the Si-C stretch at 761 cm^{-1}, and the CH_3 wag at 799 cm^{-1}. The other (1048 cm^{-1}) lies in the region of the NH_3 "umbrella" motion. We note that pairs of frequency values separated by "/" (e.g. 566/567) signify doublets, either due to nearly-degenerate modes, and/or matrix site splittings. A comparison of these product observed product bands and the corresponding M06/aug-cc-pVTZ predictions for the three predicted structures of CH_3SiCl_3–NH_3 is presented in Table 6. The predictions for methyl-equatorial geometry clearly provide the best agreement with the experimental frequencies, and that agreement is striking. The shifts predicted for the AA-short form are extreme in at least two of three cases, and for the AA-long form, the predicted shifts are slight, but in the opposite direction from what is observed. Often matrix-IR assignments are substantiated on the basis of predicted spectra shifts, which would subtract off the sometimes-large error in the absolute frequency predictions. However, in the present situation,

having chosen the M06 method on the basis of the validation against the observed bands of the parent acid fragment, not only are the shifts in agreement, the absolute frequencies agree remarkably as well. We note also that the precited value of the NH_3 "umbrella" frequency in the methyl-equatorial structure is 1041 cm^{-1}, and this only differs by 7 cm^{-1} from the observed product band in this reason (in spite of not including NH_3 frequencies in our validation). Overall, these comparisons present a reasonably-convincing case that the observed product bands arise from the methyl-equatorial form of the complex.

Table 6: A Comparison of Observed and Predicted Frequencies[a] for CH_3SiCl_3–NH_3.

Mode:	Si-Cl Assy Stretch		Si-C Stretch		CH_3 Wag	
	freq [c]	shift [d]	freq	shift [d]	freq [c]	shift [d]
Experimental [b]	567 / 566	(-8 / -9)	765	(+ 4)	810 / 816	(+11 / +15)
R-Equatorial (M06)	566 / 564	(-7 / -9)	764	(+ 5)	808 / 823	(+6 / +23)
R-Axial long (M06)	576	(+ 3)	747	(- 12)	799 / 800	(-1 / 0)
R-Axial short (M06)	500	(-73)	700	(- 59)	826 / 827	(+26 / +27)

a) Units of cm-1. b) Observed product bands in argon matrices seeded with CH_3SiCl_3 and NH_3. c) Bands denoted as pairs separated by "/" are doublets due to matrix sites or slight spittings of nearly-degenerate bands; see text for discussion.
d) Complex induced shift: ν (complex) - ν (fragment) in each case.

The situation for the CH_3GeCl_3/NH_3 matrix experiments is less clear, mainly because we observe only a few product bands, and they are observed in a very narrow range of conditions. These include a doublet at 830/846 cm^{-1}, near the CH_3 wag band of the CH_3GeCl_3 fragment, and a peak at 1008 cm^{-1}, in the NH_3 umbrella region, as well as peaks at 620, 815, and 1037/1042 that were observed only when the sample was annealed. Nonetheless, the M06 predictions for the various forms CH_3GeCl_3–NH_3 are displayed in Table 7, and there is good agreement between the predicted M06 shifts for the CH_3 wag and the pair of product bands at 830 and 846 cm^{-1}. The peaks in the NH_3 umbrella region that were observed only in annealing experiments (1037/1046) also agree with M06 predictions for the methyl-equatorial form (1046 cm^{-1}). The other peaks, that are observed only in some annealing experiments (620 and 815 cm^{-1}) seem to agree with the predicted shift of the long-bond, methyl-axial structure, as does that the 1008 cm^{-1} peak in the NH_3 umbrella region, for which the M06 prediction is

1006 cm^{-1}. These peaks, as a whole (excepting the 1008 cm^{-1}), lack the reproducibility to make any definitive statement regarding the presence the metastable, methyl-axial structure in the matrix, however, partitioning the complexes between two forms in the sample would further impede their observation. In any event, these data remain inconclusive, the reproducible product bands at 830 and 846 cm^{-1} peaks provide some firm evidence at evidence for the presence of the methyl-equatorial form in the argon-matrix environment.

Table 7: A Comparison of Observed and Predicted Frequencies[a] for CH_3SiCl_3–NH_3.

Mode:	Ge-Cl Assy Stretch		Ge-C Stretch		CH_3 Wag	
	freq [c]	shift [d]	Freq	shift [d]	freq [c]	shift [d]
Experimental [b]	-	-	620?	(-7)	830 / 846	(+9 / +25)
					815?	(- 6)
R-Equatorial (M06)	426	(-8)	627	(+ 2)	815 / 831	(+13 / +28)
R-Axial long (M06)	434	(0)	622	(- 5)	800	(-3)
R-Axial short (M06)	386	(-48)	595	(- 32)	807/808	(+4/ +5)

a) Units of cm-1. b) Observed product bands in argon matrices seeded with CH_3GeCl_3 and NH_3. c) Bands denoted as pairs separated by "/" are doublets due to matrix sites or slight spittings of nearly-degenerate bands; see text for discussion.
d) Complex induced shift: n (complex) - n (fragment) in each case.

M-N potential Curves

We also explored the M-N potentials of CH_3SiCl_3–NH_3 and CH_3GeCl_3–NH_3, mainly because of the experimental results on these systems, and in our past work, the donor-acceptor potential was key to understanding and predicting condensed-phase effects on structures. Also, because we identified equilibrium structures with distinct M-N distances for the R-axial forms of the complexes, we elected to explore the potentials of both the methyl-equatorial and methyl-axial isomers. First, we explored the method dependence for the N-Si potential of the methyl-equatorial form of CH_3SiCl_3–NH_3, and a collection of these curves is displayed in Figure 7. In addition to four DFT methods (M05, M06, M06-2X, and ω-B97X-D, all with the aug-cc-pVTZ basis set), we also obtained the CCSD/aug-cc-pVTZ energies of the M06 structures for reference (i.e. M06//CCSD). Of the various DFT methods, M06 and ω-B97X-D

track best with the CCSD energies, with M06 in slightly better agreement at the extremes of the curve, and ω-B97X-D somewhat better in the intermediate region.

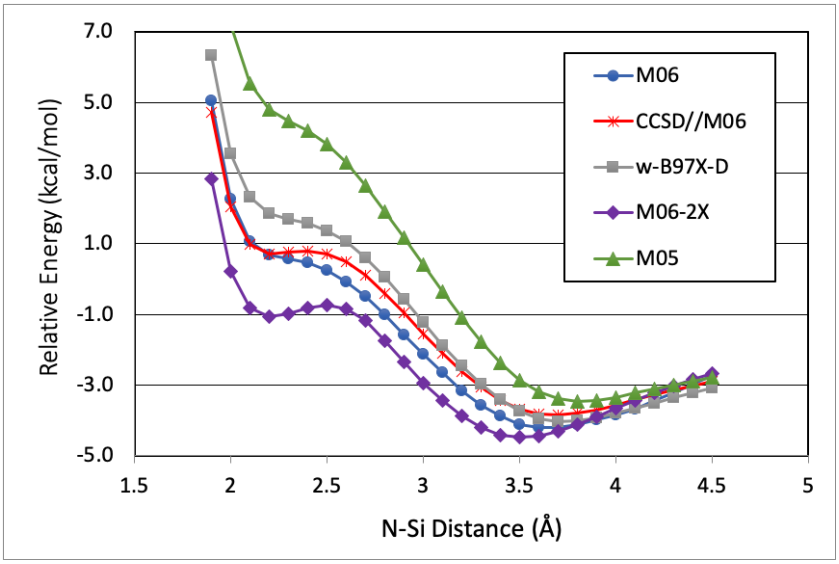

Figure 7: N-Si potential energy curves for the methyl-axial form of CH_3SiCl_3–NH_3 from four DFT methods and CCSD//M06 (as indicated) with the aug-cc-pVTZ basis set. Energies are plotted relative to the energies of the isolated fragments. All structure parameters except the fixed N-Si distance were optimized at each point on the DFT curves.

The M-N Potentials (M06/aug-cc-pVTZ) of the methyl-equatorial forms of CH_3SiCl_3–NH_3 and CH_3GeCl_3–NH_3 are displayed in Figure 8. Clearly, both curves are quite anharmonic, with a relatively slow rise inward from the equilibrium bond length. The main difference is that there is a flat, plateau-like ridge, just inside the inner wall of the curve for CH_3SiCl_3–NH_3, which is a feature we have seen previously in studies of MCl_4 complexes.[23] The curve for CH_3SiCl_3–NH_3 exhibits a long, gentle rise inward to about 2.2 Å, where the curve turns upward and the potential rises more sharply. This curve is marginally reminiscent of the weaker nitrile-BF_3 complexes, which are prone to substantial medium-induced changes in structure.[15, 40] Another more subtle difference between the curves in Figure 8 is the onset of the predominance of the repulsive forces. Surprisingly perhaps, the repulsive region for CH_3SiCl_3–NH_3 sets in at longer bond lengths than for CH_3GeCl_3–NH_3, until the innermost region of the curve, below about 2.2 Å. We presume the greater initial repulsion along this coordinate results from shorter M-Cl distances, which renders the Cl's in close proximity to the donor. But, as the acid

fragment geometry distorts to accommodate the donor-acceptor bond (at relatively short distances), the repulsions from these Cl's are reduced. At some point, a significant portion of the repulsive interaction would stem from the metal itself, and since Ge is larger than Si, that interaction would set in at longer M-N values, and thus at about 2.2 Å, the CH_3GeCl_3–NH_3 curve rises above that of its counterpart.

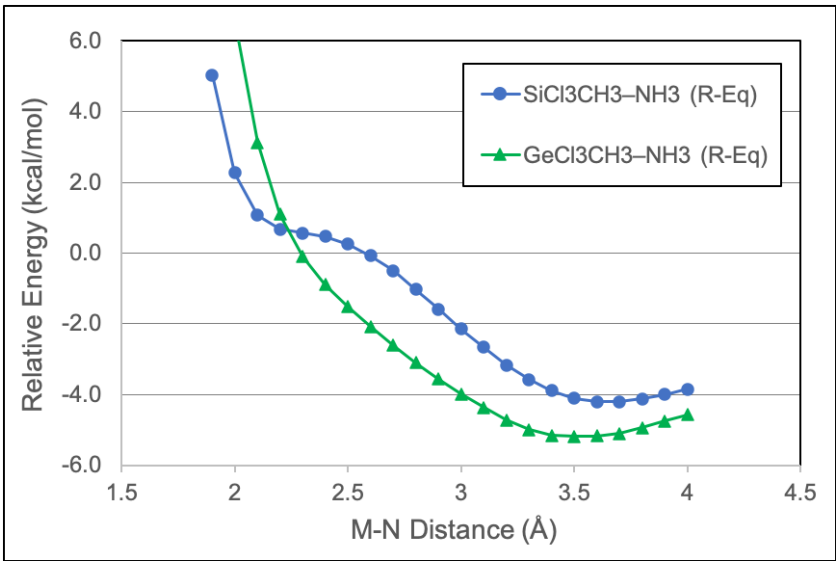

Figure 8: M-N potential energy curves for the methyl-equatorial forms of CH_3SiCl_3–NH_3 and CH_3GeCl_3–NH_3, computed via M06/aug-cc-pVTZ. Energies are plotted relative to the energies of the isolated fragments. All structure parameters except the fixed M-N distance were optimized at each point.

Another interesting feature, somewhat hidden in these data, is a continuous transition in the general structures of these complexes that takes place along this "tetrel-driven" coordinate, in which the binding seems to shift, continually, from an H-bond (CH--N) to a tetrel (N→M) interaction. For CH_3SiCl_3–NH_3, this shift takes place between 3.1 and 2.6 Å. For the transitional points in this range, the C_3 axis of the NH_3 is directed at various points along the Si-C bond, gradually shifting in its alignment from H to N through this range. At distances below 2.6 Å the interaction is clearly tetrel in nature; the NH_3 lone pair is directed at the Si. The same effect occurs along the curve for CH_3GeCl_3–NH_3, but over a slightly longer distance range, 3.3 to 2.8 Å.

The M-N potentials (M06/aug-cc-pVTZ) of the methyl-axial forms of CH_3SiCl_3–NH_3 and CH_3GeCl_3–NH_3 are displayed in Figure 6. These potentials are also quite anharmonic, and the striking feature is the occurrence of two distinct minima long these curves. These were noted a above as well, i.e., the structures associated with these minima are displayed in Figure 4. However, these plots more readily depict the relative energies of the minima, and in addition, the barriers between them are indicated. For of CH_3SiCl_3–NH_3, the "long-bond" minimum lies about 1.5 kcal/mol is lower in energy, and the barrier is about 2.1 kcal/mol (relative to the outer, global minimum). In fact, the inner minimum lies just above the energy of the separated fragments. The relative energies of the two minima on the CH_3GeCl_3–NH_3 curve are much closer in energy, and the barrier is less. Here, the long-bond minimum lies about 0.5 kcal/mol lower in energy, and the barrier is 1.4 kcal/mol. Though these methyl-axial structures are disfavored relative to their R-equatorial counterparts, our future efforts will be concerned with designing complexes for which these arrangements favored, by incorporating more electron withdrawing R-groups and less electronegative X substituents.

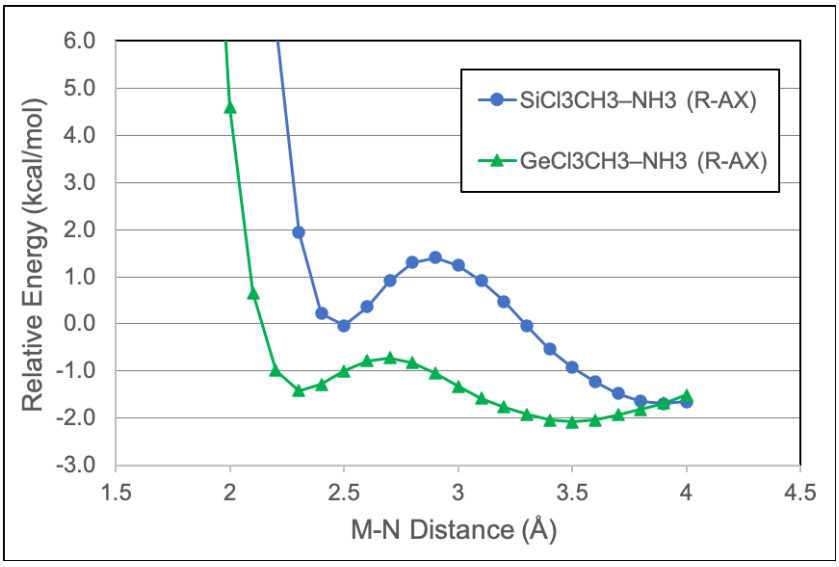

Figure 9: M-N potential energy curves for the methyl-axial forms of CH_3SiCl_3–NH_3 and CH_3GeCl_3–NH_3, computed via M06/aug-cc-pVTZ. Energies are plotted relative to the energies of the isolated fragments. All structure parameters except the fixed M-N distance were optimized at each point on the DFT curves.

Finally, we explored the effect of dielectric media on the M-N potential of the R-equatorial forms of CH_3SiCl_3–NH_3 and CH_3GeCl_3–NH_3, and a series of these curves for each complex are displayed in Figure 10. In each case, the top curve is the gas-phase potential (M06/aug-cc-pVTZ), and the curves below include the free energy of solvation as obtained by the PCM model (i.e., PCM/M06/aug-cc-pVTZ). The sum of the gas-phase fragment energies serves as the reference in these curves. Both sets of curves exhibit, in general, the response that manifests condensed-phase structural changes in donor-acceptor systems;[15] the inner regions of the curves are preferentially stabilized, and at some point, the global potential minimum shifts inwards. Here, the effect is slight at low dicentrics, and as noted above, we see no evidence of matrix-induced structural change. However, the key underlying behavior persists at higher dielectrics, despite the shifts in the interaction from at H-bonding at longer distances, to tetrel bonding at shorter distances. The curves do exhibit differences, however. For CH_3SiCl_3–NH_3 the plateau-like feature becomes a distinct minimum, and it becomes the global minimum above about e=5.0, but the barrier persists. The curve for CH_3GeCl_3–NH_3 lacks this these distinct features, but a secondary minimum develops at about 2.3 Å for e-values above about 3.0. This minimum is global in the e = 10.0 curve, and the barrier is quite subtle. Though these data only predict a contraction of the M-N bond at high dielectrics, the general response of these potentials suggests that more sensitive systems could be designed by properly altering the substituents.[15]

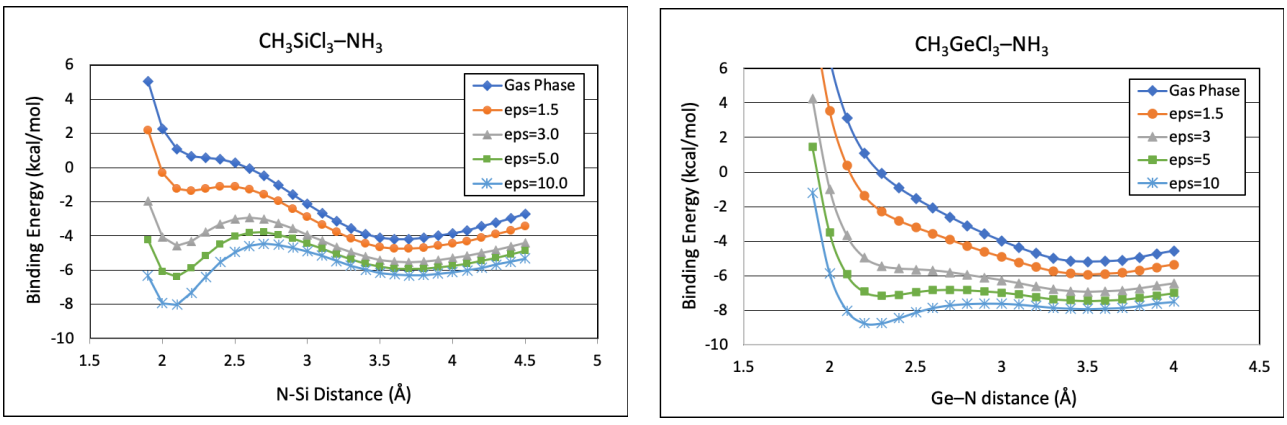

Figure 10: M-N Potential energy curves for CH_3SiCl_3–NH_3 and CH_3GeCl_3–NH_3, in the gas phase (top) and dielectric media via (PCM/M06/aug-cc-pVTZ) computations. These energies are the sum of the gas-phase electronic energy and the solvation free energy, and our plotted relative to the sum of the gas-phase fragment energies.

Summary and Conclusions

We have explored the structural and energetic properties of a series of RMX_3–NH_3 complexes (M= Si, Ge; X=F, Cl; R= CH_3, C_6H_5 (or Ph)) using primarily M06/aug-cc-pVTZ computations, with some additional insight from matrix-isolation IR spectroscopy. The minimum energy structures of these systems are the 'R-equatorial' geometries, in which the NH_3 binds axially to the halogen substituent, and the R-group resides in a equatorial site about the metal. However, with the exception of $RGeF_3$–NH_3, these complexes are weak, with binding energies of about 4-5 kcal/mol, and the acid fragments retain near-tetrahedral geometries the complexes. Furthermore, the primary interactions in the weaker systems, especially for $RMCl_3$–NH_3, seem to be weak H-bonds between the NH_3 and a hydrogen on the organic substituent (C-H--N). By contrast, the $RGeF_3$–NH_3 systems exhibit moderately strong tetrel bonds (N→Ge), with binding energies of about 9 kcal/mol and significant distortion of the acid subunit. Charge analyses and electrostatic potentials maps of the acid fragments provide a clear rationalization of these observations; the NH_3 coordinates to the most positively-charged region of the fragment in each of these minimum-energy cases.

We have also located meta-stable R-axial geometries for these systems, in which both the NH_3 and R-groups are oriented in an axial manner. These lie between 2 and 6 kcal/mol higher in energy than their R-equatorial counterparts, and the interactions are primarily of a weak tetrel-type (N→M). The charge analyses and fragment electrostatic potentials also provide a sound physical rationale for these observations; the sigma holes opposite the M-R bonds are less positively charged than those opposite the M-X bonds (or the H's on the organic group, as appropriate). One other notable feature of the R-axial geometries, in the case of in the chlorine-containing complexes, is the occurrence of distinct structures with different M-N bond distances.

Product bands observed in IR spectra of argon matrices doped with CH_3SiCl_3 and NH_3 are quite consistent with M06 frequency predictions (both shifts and actual frequency values) for the methyl-equatorial form of CH_3SiCl_3–NH_3. Analogous matrix-IR experiments with CH_3GeCl_3 and NH_3 yielded less-conclusive results. Fewer product bands were observed overall, and a few peaks were only observed in

annealing experiments. Nonetheless, two peaks were consistent with the methyl-equatorial form of CH_3GeCl_3–NH_3, yet some product bands seem to agree with M06 predictions for the 'long-bond', R-axial form of the complex. Finally, we presented pointwise (M06/aug-cc-pVTZ) maps of the M-N potential curves for both R-equatorial and R-axial forms of CH_3SiCl_3–NH_3, and CH_3GeCl_3–NH_3. These curves are remarkably anharmonic, and in the case of the R-axial geometries, highlight the occurrence of two sets of equilibrium structures, the distinct minima along the M-N coordinate, and also convey the barriers between them. For the R-equatorial geometries of CH_3SiCl_3–NH_3, and CH_3GeCl_3–NH_3, we also explored the effects of dielectric media on the M-N potential, using PCM/M06/aug-cc-pVTZ, with e =1.5 to 10. The curves at the upper end of this range of e-values indicate that the structures would change significantly in condensed-phased media, in spite of the fact that the interaction evolves from an H-bond (C---N) to a tetrel bond (N$\rightarrow$M) as the M-N coordinate is compressed. The inner regions of the potentials are flat, and preferentially stabilized via interactions with the dielectric media, which causes the global minima to shift inwards at higher e-values.

Funding Information

This work was supported by the National Science Foundation (US) Awards # CHE-1566035 (to J.A.P.), and #CHE-1626238 (MERCURY).

Research Resources

This work was made possible through a CPU time allotted through the Blugold Supercomputing Cluster (BGSC) at UW – Eau Claire.

References

1. https://www.nobelprize.org/prizes/chemistry/1969/hassel/lecture/ (accessed March 11, 2020).
2. Bent, H. A., Structural chemistry of donor-acceptor interactions. *Chemical Reviews* **1968,** *68* (5), 587-648.
3. Rose, J., *Molecular complexes*. First edition . ed.; Pergamon Press: Oxford ; New York, 1967; p x, 177 pages.
4. Mulliken, R. S.; Person, W. B., *Molecular complexes; a lecture and reprint volume*. Wiley-Interscience: New York, 1969; p xv, 498 pages.

5. Yarwood, J., *Spectroscopy and structure of molecular complexes*. Plenum Press: London ; New York, 1973; p xvii, 594 pages.
6. Foster, R., *Molecular complexes*. Crane, Russak: New York, 1973; p 2 volumes.
7. Jonas, V.; Frenking, G.; Reetz, M. T., Comparative Theoretical Study of Lewis Acid-Base Complexes of BH_3, BF_3, BCl_3, $AlCl_3$, and SO_2. *Journal of the American Chemical Society* **1994,** *116* (19), 8741-8753.
8. Frenking, G.; Wichmann, K.; Frohlich, N.; Loschen, C.; Lein, M.; Frunzke, J.; Rayon, V. M., Towards a rigorously defined quantum chemical analysis of the chemical bond in donor-acceptor complexes. *Coordination Chemistry Reviews* **2003,** *238*, 55-82.
9. Desiraju, G. R.; Ho, P. S.; Kloo, L.; Legon, A. C.; Marquardt, R.; Metrangolo, P.; Politzer, P.; Resnati, G.; Rissanen, K., Definition of the halogen bond (IUPAC Recommendations 2013). *Pure and Applied Chemistry* **2013,** *85* (8), 1711-1713.
10. Cavallo, G.; Metrangolo, P.; Milani, R.; Pilati, T.; Priimagi, A.; Resnati, G.; Terraneo, G., The Halogen Bond. *Chemical Reviews* **2016,** *116* (4), 2478-2601.
11. Grabowski, S. J., Triel bond and coordination of triel centres - Comparison with hydrogen bond interaction. *Coordination Chemistry Reviews* **2020,** *407*.
12. Bauza, A.; Mooibroek, T. J.; Frontera, A., Tetrel-Bonding Interaction: Rediscovered Supramolecular Force? *Angewandte Chemie-International Edition* **2013,** *52* (47), 12317-12321.
13. Rezac, J.; de la Lande, A., On the role of charge transfer in halogen bonding. *Physical Chemistry Chemical Physics* **2017,** *19* (1), 791-803.
14. Leopold, K. R.; Canagaratna, M.; Phillips, J. A., Partially bonded molecules from the solid state to the stratosphere. *Accounts of Chemical Research* **1997,** *30* (2), 57-64.
15. Phillips, J. A., Structural and energetic properties of nitrile-BX3 complexes: substituent effects and their impact on condensed-phase sensitivity. *Theoretical Chemistry Accounts* **2016,** *136* (1).
16. Burns, W. A.; Leopold, K. R., UNUSUALLY LARGE GAS-SOLID STRUCTURE DIFFERENCES - A CRYSTALLOGRAPHIC STUDY OF HCN-BF_3. *Journal of the American Chemical Society* **1993,** *115* (24), 11622-11623.
17. Reeve, S. W.; Burns, W. A.; Lovas, F. J.; Suenram, R. D.; Leopold, K. R., Microwave Spectrum and structure of HCN-BF_3 - An almost weakly bound complex. *Journal of Physical Chemistry* **1993,** *97* (41), 10630-10637.
18. Phillips, J. A.; Halfen, J. A.; Wrass, J. P.; Knutson, C. C.; Cramer, C. J., Large gas-solid structural differences in complexes of haloacetonitriles with boron trifluoride. *Inorganic Chemistry* **2006,** *45* (2), 722-731.
19. Eigner, A. A.; Rohde, J. A.; Knutson, C. C.; Phillips, J. A., IR spectrum of CH_3CN-BF_3 in solid neon: Matrix effects on the structure of a Lewis acid-base complex. *Journal of Physical Chemistry B* **2007,** *111* (6), 1402-1407.
20. Grabowski, S. J., pi-Hole Bonds: Boron and Aluminum Lewis Acid Centers. *Chemphyschem* **2015,** *16* (7), 1470-1479.
21. Buchberger, A. R.; Danforth, S. J.; Bloomgren, K. M.; Rohde, J. A.; Smith, E. L.; Gardener, C. C. A.; Phillips, J. A., Condensed-Phase Effects on the Structural Properties of FCH_2CN–BF_3 and $ClCH_2CN$–BF_3: A Matrix-Isolation and Computational Study. *Journal of Physical Chemistry B* **2013,** *117* (39), 11687–11696.

22. Phillips, J. A.; Cramer, C. J., B-N distance potential of CH_3CN-BF_3 revisited: Resolving the experiment-theory structure discrepancy and modeling the effects of low-dielectric environments. *Journal of Physical Chemistry B* **2007,** *111* (6), 1408-1415.
23. Helminiak, H. M.; Knauf, R. R.; Danforth, S. J.; Phillips, J. A., Structural and Energetic Properties of Acetonitrile-Group IV (A & B) Halide Complexes. *Journal of Physical Chemistry A* **2014,** *118* (24), 4266-4277.
24. Waller, A. W.; Weiss, N. M.; Decato, D. A.; Phillips, J. A., Structural and energetic properties of haloacetonitrile - GeF_4 complexes. *Journal of Molecular Structure* **2017,** *1130*, 984-993.
25. Waller, A. W., Honors Manuscript, UWEC Chemistry, 2015. .
26. Hora, N. J.; Wahl, B. M.; Soares, C.; Lara, S. A.; Lanska, J. R.; Phillips, J. A., On the interactions of nitriles and fluoro-substituted pyridines with silicon tetrafluoride: Computations and thin film IR spectroscopy. *Journal of Molecular Structure* **2018,** *1157*, 679-692.
27. Donald, K. J.; Tawfik, M., The Weak Helps the Strong: Sigma-Holes and the Stability of MF_4 center dot Base Complexes. *Journal of Physical Chemistry A* **2013,** *117* (51), 14176-14183.
28. Donald, K. J.; Befekadu, E.; Prasad, S., Coordination and Insertion: Competitive Channels for Borylene Reactions. *Journal of Physical Chemistry A* **2017,** *121* (46), 8982-8994.
29. Politzer, P.; Murray, J. S.; Clark, T.; Resnati, G., The sigma-hole revisited. *Physical Chemistry Chemical Physics* **2017,** *19* (48), 32166-32178.
30. Clark, T.; Hennemann, M.; Murray, J. S.; Politzer, P., Halogen bonding: the sigma-hole. *Journal of Molecular Modeling* **2007,** *13* (2), 291-296.
31. Brinck, T.; Borrfors, A. N., Electrostatics and polarization determine the strength of the halogen bond: a red card for charge transfer. *Journal of Molecular Modeling* **2019,** *25* (5).
32. Frisch, M. J.; Trucks, G. W.; Schlegel, H. B.; Scuseria, G. E.; Robb, M. A.; Cheeseman, J. R.; Scalmani, G.; Barone, V.; Mennucci, B.; Petersson, G. A.; *al., e.*
33. Giesen, D. J.; Phillips, J. A., Structure, bonding, and vibrational frequencies of CH_3CN-BF_3: New insight into medium effects and the discrepancy between the experimental and theoretical geometries. *Journal of Physical Chemistry A* **2003,** *107* (20), 4009-4018.
34. Cramer, C. J., *Essentials of computational chemistry: theories and models*. Wiley. com: 2005.
35. Zhao, Y.; Truhlar, D. G., Density functionals with broad applicability in chemistry. *Accounts of Chemical Research* **2008,** *41* (2), 157-167.
36. Chai, J. D.; Head-Gordon, M., Long-range corrected hybrid density functionals with damped atom-atom dispersion corrections. *Physical Chemistry Chemical Physics* **2008,** *10* (44), 6615-6620.
37. Weinhold, F.; Landis, C. R., *Discovering chemistry with natural bond orbitals*. Wiley: Hoboken, NJ, 2012; p xii, 319 p.
38. Reed, A. E.; Weinstock, R. B.; Weinhold, F., Natural population analysis. *Journal of Chemical Physics* **1985,** *83* (2), 735-746.
39. Wrass, J. P.; Sadowsky, D.; Bloomgren, K. M.; Cramer, C. J.; Phillips, J. A., Quantum chemical and matrix-IR characterization of CH_3CN-BCl_3: a complex with two distinct minima along the B-N bond potential. *Physical Chemistry Chemical Physics* **2014,** *16* (31), 16480-16491.
40. Phillips, J. A.; Danforth, S. J.; Hora, N. J.; Lanska, J. R.; Waller, A. W., Structural and Energetic Properties of Haloacetonitrile-BCl_3 Complexes: Computations and Matrix-IR Spectroscopy. *Journal of Physical Chemistry A* **2017,** *121* (48), 9252-9261.

41. Mantina, M.; Chamberlin, A. C.; Valero, R.; Cramer, C. J.; Truhlar, D. G., Consistent van der Waals Radii for the Whole Main Group. *Journal of Physical Chemistry A* **2009,** *113* (19), 5806-5812.
42. Smith, E. L.; Sadowsky, D.; Phillips, J. A.; Cramer, C. J.; Giesen, D. J., A Short Yet Very Weak Dative Bond: Structure, Bonding, and Energetic Properties of N_2-BH_3. *Journal of Physical Chemistry A* **2010,** *114* (7), 2628-2636.